Organization of the magnetosphere during substorms

T. Živković,[1] and K. Rypdal,[1]

Abstract. The change in degree of organization of the magnetosphere during substorms is investigated by analyzing various geomagnetic indices, as well as interplanetary magnetic field z-component and solar wind flow speed. We conclude that the magnetosphere self-organizes globally during substorms, but neither the magnetosphere nor the solar wind become more predictable in the course of a substorm. This conclusion is based on analysis of five hundred substorms in the period from 2000 to 2002. A minimal dynamic-stochastic model of the driven magnetosphere that reproduces many statistical features of substorm indices is discussed.

1. Introduction

The complexity of the magnetosphere has been extensively studied and one of its descriptions is based on the paradigm of self-organized criticality (SOC) coined by *Bak et al.* [1987]. Systems that exhibit SOC activate many degrees of freedom, their interactions are local, but due to the excitation of a scale-free hierarchy of avalanches when the system is slowly driven to a criticality threshold, long-range interactions develop, and the dynamics on different spatial and temporal scales is essentially the same. It has been shown that the magnetospheric-ionospheric system exhibit signatures characteristic of SOC-dynamics [*Vörös*, 1991], [*Uritsky and Pudovkin*, 1998] and models for such description have been developed [*Chapman et al.*, 1998; *Chang*, 1999; *Uritsky et al.*, 2002; *Kozelov and Kozelova*, 2003]. On the other hand, the magnetospheric-ionospheric system has also some signatures of intermittent turbulence [*Golovchanskaya et al.*, 2008], non-equilibrium phase-transitions [*Sitnov et al.*, 2001] as well as low-dimensional chaos [Sharma et al., 1993]. It has been recently reported in *Živković and Rypdal* [2011] that the magnetosphere, interplanetary magnetic field (IMF) z-component B_z and solar wind flow speed v become more predictable and more persistent during magnetic storms, while only the magnetosphere reduces the effective number of degrees of freedom through self-organization. In that study the magnetosphere was studied through analysis of the geomagnetic indices SYM-H and D_{st}, since it is known that these indices respond to the intensification of the ring current during magnetic storms [*Wanliss*, 2006]. In this article we analyze how different magnetospheric indices respond to the much more frequent and short-living events called substorms.

Different geomagnetic indices represent different parts of the magnetosphere and respond to different dynamics. The most commonly used index for substorm studies is the Kyoto auroral electrojet index (AE) minute data defined as the difference between the AU index, which measures the strength of the eastward electrojet in the auroral zone, and the AL index, measuring the westward electrojet current, and is usually derived from 12 magnetometers positioned below the auroral oval [*Davies and Sugiura*, 1966]. We also use minute data for the IMF component B_z, as well as minute data for the solar wind bulk velocity v along the Sun-Earth axis. They are both retrieved from the OMNI satellite database and are given in GSE coordinate system.

[1]Department of Physics and Technology, University of Tromsø, Norway.

0148-0227/11/$9.00

We have not analyzed other plasma parameters, since the plasma instruments can be influenced by solar X rays or energetic particle precipitation and are more unstable than the magnetometers. We also analyze the polar cap magnetic activity (PC), as well as the AU and the AL index. During magnetically disturbed times the westward electrojet, whose proxy is the AL index, increases abruptly due to currents from the magnetotail. On the other hand, the eastward electrojet, whose proxy is the AU index, increases due to the partial ring current closure via the ionosphere in the evening sector [*Feldstein et al.*, 2006]. Therefore, through the analysis of the AL and AU index we can get the insight into the dynamics of different parts of the magnetosphere. The PC index monitors geomagnetic activity over the polar caps caused by changes in the IMF and the solar wind. This index is mostly influenced by field-aligned currents which flow at the poleward rim of the auroral oval, and is also sensistive to the ionospheric Hall currents in the polar cap [*Vennestrøm et al.*, 1991], which are particularly dominant in the summer time. Since field-aligned currents are closely related to the auroral electrojets, the linear correlation of the PC and AE indices is of the order of 0.8-0.9 [*Vennestrøm et al.*, 1991]. Here we use the northern polar cap index measured at the Danish geomagnetic observatory in Thule (86.5°N).

Magnetic substorms are associated with release and storage of energy and momentum from the solar wind to the magnetosphere. They consist of three phases. In the growth phase, typically lasting for about one hour, loading of the magnetic flux and energy into the magnetotail takes place. It is succeeded by the expansion phase (substorm onset), lasting 30-60 minutes, when hot plasma "unloads" earthward, leading to sudden brightenings of the polar aurora. In this phase dissipation is dominant and formation of a storm ring current can take place. In the ionosphere substorm onset is characterized by a rise of the westward electrojet current, which forms the substorm current surge with field aligned currents. The recovery phase returns the magnetosphere to its quiet state. The duration of this this phase is 1-2 hours.

Data about the times of substorm onsets are found in *Frey et al.* [2004], whose database is from the period between 2000 and 2002. These substorms were detected by the FUV instrument on the IMAGE spacecraft. Observations covered the peak of the last solar cycle. According to *Frey et al.* [2004] a substorm onset is only accepted as a separate event if at least 30 minutes have passed after the previous event. It is also required that local brightening of aurora occurs and that the aurora expands to the poleward boundary of the auroral oval and spreads azimuthally in local time for at least 20 minutes. The latter criterion excludes pseudo-breakups which do not develop into full substorms.

The remainder of the paper is organized as follows: section 2 gives a brief overview of the methods used in the analysis of our data. Section 3 shows the results from application of these methods to the substorm data and section 4 is reserved for discussion.

2. Methods

This paper is a continuation of our paper on magnetic storms [*Živković and Rypdal*, 2011], where organization and persistence in the solar wind and the magnetosphere were studied under storm conditions. A more thorough description of the methods outlined in this section is presented there.

2.1. Recurrence-plot analysis

Recurrence-plot analysis was developed by *Eckmann et al.* [1987] and is very useful in studies of short and non-stationary time series. Recurrence plots are based on the recurrences of a trajectory $\mathbf{z}(t)$ on the d-dimensional attractor in a $p > d$-dimensional phase space. Provided that the attractor of the dynamical system has dimension d, Takens' time-delay method [*Takens*, 1981] can be used to construct an $m > 2d$-dimensional embedding space on which the attractor can be mapped continuously and one-to-one. The embedding space is constructed from the time series $x_i = g(\mathbf{z}(i\,\delta t))$, where $g(\mathbf{z})$ is the measurement function. Here $t = i\,\delta t$, and δt is the sampling time of the time series. The mapping is given by

$$\mathbf{x}_i = (x_i, x_{i+\tau}, \ldots, x_{i+(m-1)\tau}), \tag{1}$$

where τ is the time delay. Recurrence in embedding space occurs when the distance $\|\mathbf{x}_i - \mathbf{x}_j\| < \epsilon$, where ϵ is the cut-off distance, and $i, j = 1 \ldots N$. Further, an $N \times N$ matrix $\mathbf{R}$ is computed, whose elements are $R_{i,j} = 1$ when recurrence takes place and $R_{i,j} = 0$ otherwise.

Substorm durations are at most a few hours and all indices show non-stationary behavior during the events. Recurrence-plot analysis is very suitable for handling such short non-stationary time series. Of particular interest is analysis based on the diagonal line structures of the recurrence plots. We use the average inverse diagonal line length Γ:

$$\Gamma \equiv \langle l^{-1} \rangle = \sum_l l^{-1} P(l) / \sum_l P(l), \tag{2}$$

where $P(l)$ is a histogram over diagonal lengths:

$$P(l) = \sum_{i,j=1}^{N} (1 - R_{i-1,j-1})(1 - R_{i+l,j+l}) \prod_{k=0}^{l-1} R_{i+k,j+k}. \tag{3}$$

It has been shown heuristically in *Živković and Rypdal* [2011] that Γ can be used as a proxy for the largest Lyapunov exponent in deterministic systems and as a measure of persistence in stochastic systems. For the latter, *Živković and Rypdal* [2011] derived a relation between Γ and the self-similarity exponent h, which can be defined for self-similar time series; $\Gamma = 0.72 - 0.56\ (2h)$. This relation is valid for persistent Gaussian motions. Therefore, we use Γ as a measure of predictability in the system, since decrease in Γ means decrease in Lyapunov exponent for a deterministic system or increase in persistence for a stochastic system.

2.2. A test for determinism

This test was developed by *Kaplan and Glass* [1992]. It takes advantage of the fact that a deterministic dynamical system with state vector $\mathbf{z}$ evolves according to an autonomous equation of the form

$$\frac{d\mathbf{z}}{dt} = \mathbf{f}(\mathbf{z}). \tag{4}$$

This implies that the space trajectory through a given point in phase space is completely determined by this position, and if a trajectory recurs to the vicinity of this point the tangents of the trajectory in these two points are approximately parallel. This is in contrast to a stochastic system, where the directions of the tangents are independent for the two points. Let us assume that the phase space is divided into boxes. In our test, a box size is chosen as the average distance a phase-space point moves in the m-dimensional embedding space during one time step. The displacement of the trajectory inside a box, in m-dimensional phase space is given from the time-delay embedding reconstruction:

$$\begin{aligned}\Delta\mathbf{x}(t) \;=\; & [x(t+b) - x(t), x(t+\tau+b) - x(t+\tau), \ldots, \\ & x(t+(m-1)\tau+b) - x(t+(m-1)\tau)],\end{aligned} \tag{5}$$

where b is the characteristic time the trajectory spends inside a box. The tangent for the kth pass through box j is the unit vector $\mathbf{u}_{k,j} = \Delta\mathbf{x}_{k,j}(t)/|\Delta\mathbf{x}_{k,j}(t)|$. The averaged tangent in the box is

$$\mathbf{V}_j = \frac{1}{n_j} \sum_{k=1}^{n_j} \mathbf{u}_{k,j}, \tag{6}$$

where n_j is the number of passes of the trajectory through box j. In the case of deterministic dynamics and finite box size, $\mathbf{V}_j$ will not depend very much on the number of passes n_j, and V_j will converge to 1. In contrast, for the trajectory of a random process, V_j will decrease with n_j as $V_j \sim n_j^{-1/2}$. Thus, to obtain better statistics for the description of average tangents we compute the average V_j as a function of the number of passes through a box:

$$L_n \equiv \langle V_j \rangle_{n_j = n}, \tag{7}$$

where this average is done over all boxes with same number n of trajectory passes.

The test for low-dimensionality employed in this paper takes advantage of how the measure of determinism, the curves L_n, changes when we construct a new surrogate time series for which the effect of nonlinearity in a low-dimensional system has been corrupted. This surrogate signal has the same power spectral density (and hence same auto-covariance) as the original signal, but the phases of the Fourier coefficients have been randomized. From application of this procedure to synthetic stochastic and low-dimensional signals we have gained support for the conjecture that randomization of phases do not change these

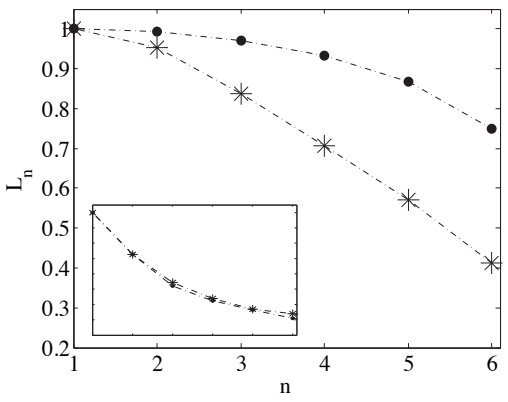

Figure 1. Mean vector length L_n vs. number of passages n: bullets are derived from numerical solutions to the MG equation, stars are derived from these solutions after randomization of phases of Fourier coefficients. Inset in the figure shows same characteristics for the fO-U process.

curves for neither stochastic or high-dimensional, nor low-dimensional and linear systems. Only for low-dimensional and nonlinear systems will the surrogate data curves lie below those based on the original data. These features were demonstrated for numerical solutions of the Lorenz system (low-dimensional, nonlinear and chaotic) in *Živković and Rypdal* [2011]. Here we demonstrate the same for L_n versus n for the Mackey-Glass (MG) equation *Mackey and Glass* [1977]:

$$\frac{dx}{dt} = -bx(t) + a\frac{x(t-\delta)}{1+x(t-\delta)^c} \tag{8}$$

Unlike the Lorenz system, the attractor of this system is in general high-dimensional. However, for some set of parameters, e.g. $a = 0.2, b = 0.1, \delta = 100, c = 10$, the attractor of MG dynamics can be low-dimensional and L_n derived from the MG equation will fall more slowly with increasing n than that for the randomized version, as shown in Figure 1. The inset in the same figure shows the same results for a fractional Ornstein-Uhlenbeck (fO-U) stochastic process. The stochastic equation used to generate such a process was described in [*Živković and Rypdal*, 2011]. The equation used to generate Figure 1 has coefficients which are generated from the AE index by means of least square regression. Realizations of a stochastic process like this is indistinguishable from realizations of a measurement function of a high-dimensional deterministic system for which the embedding dimension is too small to unfold the attractor. The L_n-curve for the fO-U process is unchanged after randomization of phases, and shows that this test for determinism is negative for stochastic (and high-dimensional) systems. This serves as a justification for considering this as a useful test for low-dimensional dynamics.

3. Results

In *Rypdal and Rypdal* [2010a] it was shown that the fluctuation amplitude (or more precisely; the one-timestep increment) $\Delta y(t)$ of the AE index is on the average proportional to the instantaneous value $y(t)$ of the index. This gives rise to a special kind of intermittency associated with multiplicative noises, and leads to a non-stationary time series of increments. However, the time series $\Delta y(t)/y(t)$ is stationary, implying that the stochastic process $x(t) = \log y(t)$ has stationary increments. Thus, a signal with stationary increments, which still can exhibit a multifractal intermittency, can be constructed by considering the logarithm of the AE index. We use transformed versions of geomagnetic indices: tAE= log(AE), tAL= log(0.1928 |AL| + 10.50), tAU=log(0.1167 |AU| + 13.50), tPC= log(0.0503 |PC| + 0.1978), while B_z and v have increments which are not strongly dependent on their magnitude, and do not need transformation to obtain stationary increments.

It is well known that the AE index exhibits stochastic characteristics since its power spectral density has two distinct power-law regimes [*Tsurutani et al.*, 1990]. However,

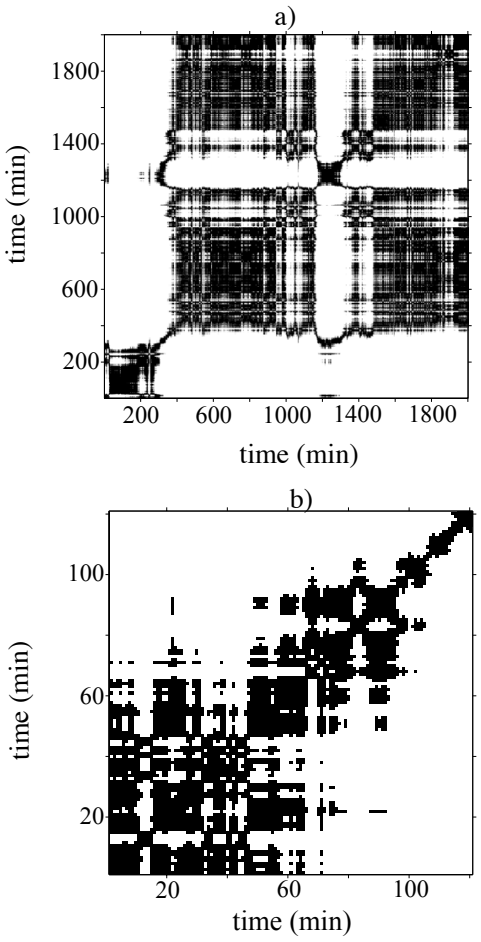

Figure 2. Recurrence plots for tAE: a) for the entire day of September 8th, 2002, containing two distinct substorms (white bands in the plot). b) Plot for the second substorm.

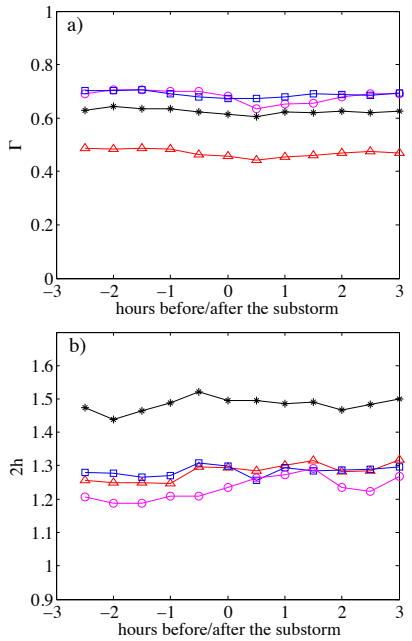

Figure 3. a) Ensemble mean of Γ averaged over 500 substorms. The standard deviations over the substorm ensemble are $\sigma(\Gamma_{tAE}) \sim 0.3$, $\sigma(\Gamma_{tAU}) \sim 0.15$, $\sigma(\Gamma_{tAL}) \sim 0.15$, and $\sigma(\Gamma_{tPC}) \sim 0.15$. b) Ensemble mean of $2h$. Standard deviations are $\sigma(h_{tAE}) \sim 0.3$, $\sigma(h_{tAU}) \sim 0.3$, $\sigma(h_{tAL}) \sim 0.35$, and $\sigma(h_{tPC}) \sim 0.25$. Triangles represent tAE, squares tAU, stars tPC, and circles tAL.

it has also been shown that apart from colored noise which dominates the dynamics of the AE index on time scales up to 100 minutes, there are also signatures of low-dimensional, chaotic characteristics as well [*Athanasiu and Pavlos*, 2001]. These properties will be discerned from the analysis of determinism of geomagnetic indices in section 3.2.

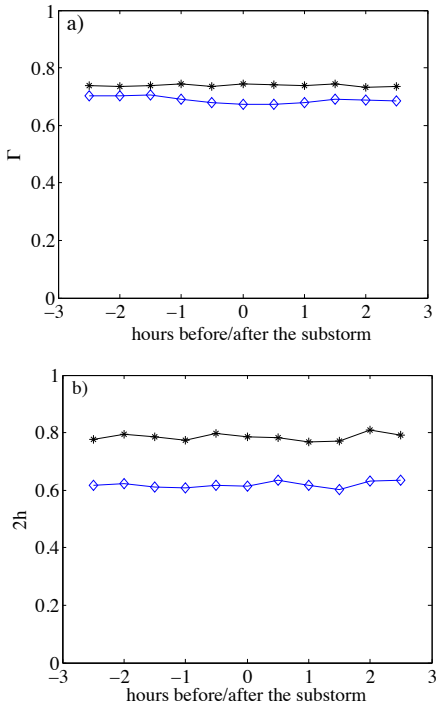

Figure 4. a) Ensemble mean for Γ. b) Ensemble mean for $2h$. Stars represent B_z and diamonds v. Standard deviation for Γ is of the order of magnitude 0.15, while for $2h$ is 0.3.

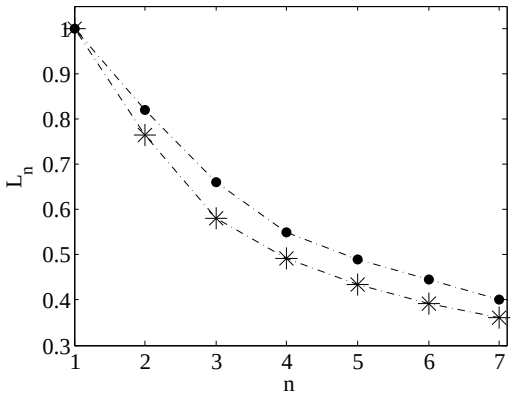

Figure 5. Mean vector length L_n vs. number of passages n: bullets are derived from the entire tAE time series, stars from this time series after randomization of phases of the Fourier coefficiens.

3.1. Predictability analysis

First, we discuss two magnetic substorms that occurred on September 8th, 2002. The first substorm onset was registered at 5:01UT and the other at 21:26 UT. The second substorm onset started after 13 hours of northward IMF B_z. In Figure 2a white bands in the recurrence plot indicate changes in the dynamics. The first white band occurs around the first substorm onset. The next appears during the second substorm. Figure 2b contains the recurrence plot for the second substorm. The image pales away from the main diagonal, which indicates that the process is nonstationary due to the intensification and the movement of ionospheric currents during the substorm. Since the plot pattern changes during the substorm we might expect that Γ, which is defined from the diagonal lines of the plot, will change as well. We compute Γ for embedding dimension $m = 1$, since stochastic dynamics of tAE is high-dimensional and cannot be unfolded in any embedding space and since Γ seems independent of m. We obtain Γ for tAE, tAU, tPC, tAL, B_z, and v for 500 substorms whose onsets were taken from the database of *Frey et al.* [2004]. The variation of Γ over a 6 hour time interval three hours before and three hours after the substorm, is computed from recurrence plots derived from thirty-minute windows, such that 12 Γ-values are obtained for each substorm. The time evolution of Γ is computed for all 500 substorms and averaged. The results are presented in Figure 3a. Apparently, there is no significant variation of the ensemble average of Γ over the duration of a substorm for any of the geomagnetic indices.

On time scales less than 100 minutes all quantities analyzed can be modeled as nonstationary multifractal motions

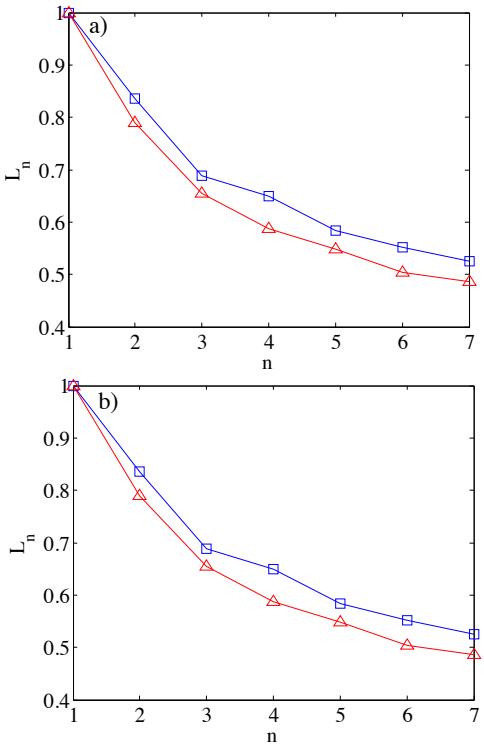

Figure 6. L_n vs. n, a) squares are derived from tAE during substorms, triangles from the entire tAE time series, b) squares from tAU during substorms, triangles from entire tAU time series.

whose persistence can be characterized by an exponent h [*Rypdal and Rypdal*, 2010a, b]. Increasing h implies higher persistence and predictability, correponding to a reduction of Γ. Figure 3b shows no variation in ensemble mean of $2h$ for any of the indices, confirming the result obtained for Γ.

The same analysis is done for B_z and v. Mean values for Γ and $2h$ are plotted in Figure 4, showing no significant change of predictabilty during substorms for the solar wind observables. The example of two substorms from September, 8th, 2002 shows a reduction of Γ around substorm onset (not shown here), but this day seems to be an exception rather than the rule.

3.2. Determinism analysis

The signals we study are dominated by a stochastic component and their L_n decreases when number of passes n is increased. However, the existence of a low-dimensional component in e.g. the AE index can be demonstrated by computing L_n and then do the same for the surrogate signals

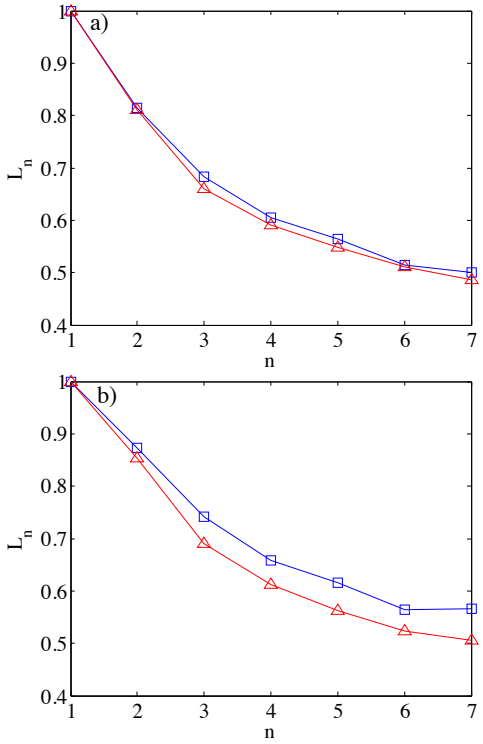

Figure 7. L_n vs. n, a) squares are derived from tAL during substorms, triangles from the entire tAL time series, b) squares from tPC during substorms, triangles from entire tPC time series.

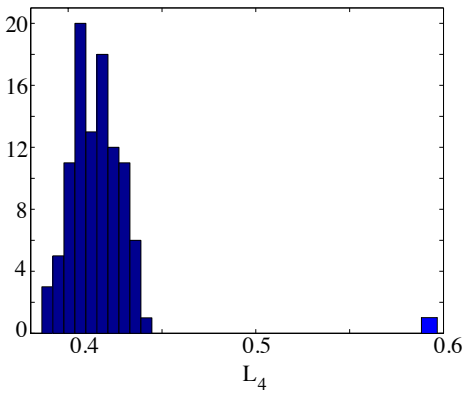

Figure 8. Histogram of L_4 derived from a hundred realizations of fO-U. Distant square is L_4 derived from tAE time series during substorm.

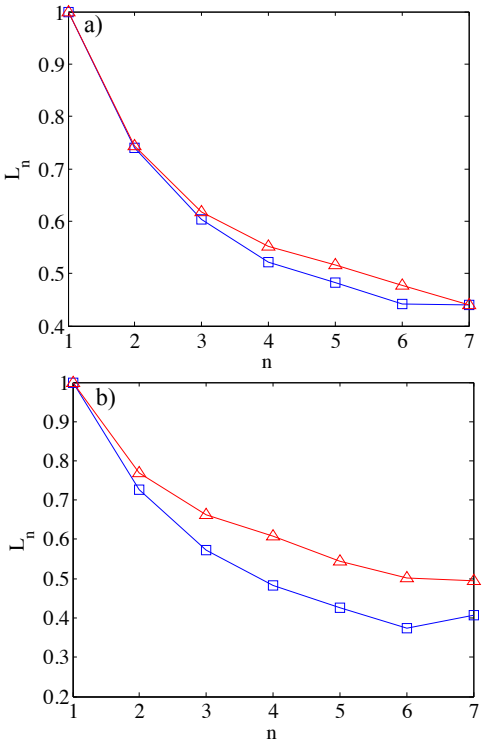

Figure 9. L_n vs. n, a) squares are derived from B_z during substorms, triangles from entire B_z time series, b) squares are derived from v during substorms, triangles from entire v time series.

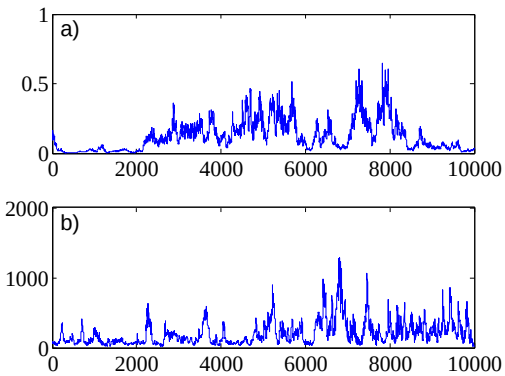

Figure 10. a) Numerical solutions of equation (10), b) AE index.

obtained by randomizing phases of Fourier coefficients. As observed in Figure 5, L_n for tAE is higher than for the randomized version, indicating existence of a low-dimensional and nonlinear component in the signal. The same test was done for the geomagnetic index SYM-H in *Živković and Rypdal* [2011], and even though analysis of this index yields low-dimensionality during magnetic storms, L_n is indistinguishable from its randomized version when averaged over a year.

As we shall demonstrate below tAE, tAU, tAL and tPC all exhibit low-dimensionality during substorms. Since substorms occur very often, sometimes several per day, this low-dimensionality is discernible also when averaged over the year. We use the substorm database and compute L_n in the time interval one hour before and two hours after the substorm onset. This way we generally include all phases of the substorm. This analysis is made for tAE, tAL, tAU, and tPC, and compared to L_n computed from all the data from year 2000. Figures 6 and 7 illustrate that all geomagnetic indices (except tAL) exhibit elevated determinism during substorm times, i.e. low-dimensionality increases during substorms.

Another way to demonstrate the existence of a low-dimensional component in these indices is to compare the determinism computed from the AE index during substorms with signals generated numerically from the fO-U equation. For each of a hundred realizations of the fO-U process, we compute L_4 as a measure of low-dimensionality. From L_4 one can distinguish between stochastic and deterministic systems, since $L_4 \sim 1$ for the Lorenz system and $L_4 \sim 0.4$ for a Gaussian noise. In figure 8 we plot a histogram of L_4 for the fO-U realizations and tAE under substorm condition. L_4 for tAE is far out of the range of L_4 produced for hundred realizations of fO-U, showing that determinism in tAE is significantly higher than for the modeled stochastic signal.

In Figure 9 we plot L_n for B_z and v, and observe some *reduction* in determinism (stronger in v than in B_z) during substorms. This indicates that the increased low-dimensional component in the geomagnetic indices during substorms is not imposed on the magnetosphere by the growth of such a component in the solar wind. In other words: the organization of the magnetosphere during substorms is a *self*-organization.

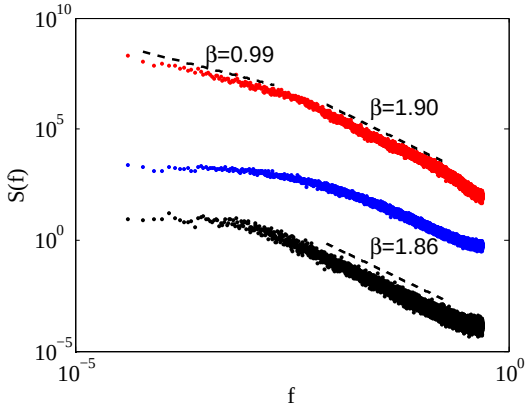

Figure 11. Power spectral denities. Upper curve: from AE index. Middle: from solutions of equation (10) with w a fractional Gaussian noise with $H = 0.45$. Lower: from fO-U process with w the same as above.

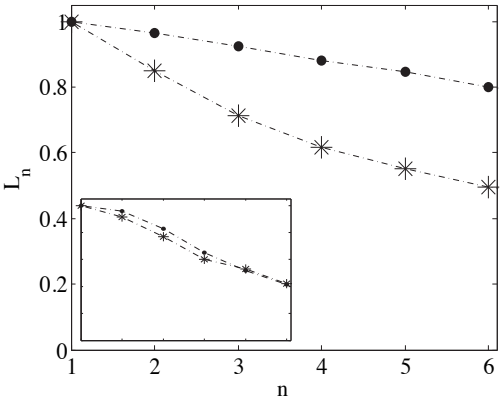

Figure 12. Mean vector length L_n vs. number of passages n: bullets are derived from low-pass filtered numerical solutions to equation (10), stars are derived from these solutions after randomization of phases of Fourier coefficients. Inset in the figure shows same characteristics for the filtered fO-U process.

4. Discussion

We have applied recurrence-plot analysis and a test of determinism to geomagnetic indices AE, AU, AL and PC, as well as IMF B_z and solar flow speed v. Recurrence plots were applied by *March et al.* [2005a] to connect solar wind observables to the AL and AU indices, concluding that the correlation between these indices results from magnetic storm signatures appearing in both time series. Also, correlation between the solar wind electric field vB_z and the AE index was studied in *March et al.* [2005b], invoking mutual information. Here it was found that correlation is present intermittently on the timescales of a few hours, suggesting that substorms are information carriers between the solar wind and the magnetosphere. In our study, recurrence analysis is used to measure the inverse average diagonal line length Γ which is heuristically shown to be a useful measure of predictability of the dynamics. As an alternative predictability measure the self-similarity exponent h was measured during the course of substorms. No systematic variation of h or Γ

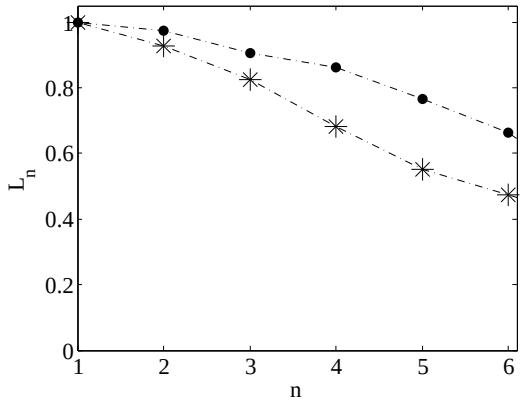

Figure 13. Mean vector length L_n vs. number of passages n: bullets are derived from the entire low-pass filtered tAE time series, stars from this time series after randomization of phases of the Fourier coefficiens.

during substorms has been detected in an ensemble of five hundred substorms. This is true both for geomagnetic indices and the solar wind observables. Thus we conclude that geomagnetic indices which represent dynamics in the magnetotail, plasma sheet boundary layer, partial ring current and polar cap convection, do not become more predictable during substorms. The same applies for observables representing the dynamical state of the solar wind driver.

A simple test for determinism has shown that the AE index exhibits some low-dimensional and nonlinear characteristics, which are elevated during substorms. Other geomagnetic indices also get more deterministic during magnetic substorms, which could indicate that the entire magnetosphere self-organizes and develops low-dimensional dynamics under substorm conditions. For the AE index similar results were obtained by *Athanasiu and Pavlos* [2001], who applied singular value decomposition (SVD) analysis to the AE index. They concluded, by comparing the AE index with solutions of the Lorenz system contaminated by a colored noise term, that the first SVD component in both cases is entirely due to colored noise, while the higher order SVD components are due to the internal, low-dimensional and chaotic dynamics. By computing cross-correlation between the first SVD component of the AE index and the index itself, they concluded that the influence of the first component is about 40 percent. Further, the first SVD component is attributed to the solar wind and is characterized as linear and stochastic, while higher SVD components are attributed to magnetospheric dynamics. In our test of determinism the data are not filtered to reduce the effect of the stochastic component on the analyis, but the results still reveal that unlike IMF B_z, the AE index contains components that make it different from a linear, stochastic system.

Thus, it seems firmly established that the auroral electrojet proxies exhibit an additional low-dimensional component associated with self-organization of the magnetosphere, the most prominent example being the auroral substorm. It should be stressed, however, that also for AE activity the *major* component is stochastic. *Chapman and Watkins* [2001] argue that the AE index contains information transferred from the solar wind, since it has been shown in *Freeman et al.* [2000] that power laws in burst lifetime distribution for the AL and AU indices and for the solar wind electric field vB_z are similar apart from a bump in the lifetime distribution which *Freeman et al.* [2000] explain as a signature of the substorm current system. This indicates that the stochastic component of the auroral electrojet activity to a great extent is a direct imprint of the solar wind turbulence. This conclusion is supported by the analysis in *Rypdal and Rypdal* [2010b], where B_z and tAE are found to exhibit very similar multifractal spectrum on the time scale up to 100 minutes.

Our analysis supports a picture where the magnetosphere under quiet conditions resides in a forced state where the organization of the magnetospheric dynamics to a great extent reflects the organization of the solar wind driver, i.e. the stochastic properties of the global magnetospheric system and the driver are very similar. If substorms are trigged by solar wind features, this trigger is not an increase in organization or predictability of the solar wind dynamics. During substorms all geomagnetic indices analyzed are influenced by a self-organization that involves the major current systems in the magnetosphere-ionosphere, and hence indicates that a global instability is exited. This picture is consistent with the scenario described in *Chang* [1999], and conceptually simpler forerunners like *Lewis* [1991]. The latter sets out to explain the unpredictability of substorm onset, noting that external triggers, like reversal from northward to southward pointing B_z, are not always identifiable, and series of substorm cycles can occur if southward IMF persists for prolonged times. Southward IMF opens up for loading of magnetic flux and energy to the magnetosphere, and in *Lewis* [1991], and further elaborated by *Sitnov et al.* [2001], parameters representing this loading are modeled as external time-dependent control parameters, and the magnetospheric state-variable (e.g. a geomagnetic index) is modeled via a non-autonomous system on the form

$$\frac{dX}{dt} = F(X, a, b), \tag{9}$$

where $a(t)$, $b(t)$ are two time-dependent external control parameters. The underlying assumption is that the magnetosphere resides in a forced equilibrium corresponding to a stable fixed point of this system, and hence these equilibria are located on the surface $F(X, a, b) = 0$ in the three-dimensional (X, a, b)-space. Choosing a third-order polynomial form, e.g. $F(X, a, b) = X^3 + aX + b$, gives rise to a folded surface that opens the possibility of a cusp catastrophe which is interpreted as the substorm onset (expansion phase). According to this non-autonomous model for evolution of stable, forced equilibria the substorm onset is not really unpredictable since it depends on the control parameters a and b. However, the catastrophe can occur along a curve in the (a, b)-plane which may be hard to identify from this kind of conceptual model, and hence practical prediction may be difficult.

One unsatisfactory feature of non-autonomous models of this kind is that the control parameters are not directly related to the state of the solar wind driver, but rather a result of the solar-wind/magnetosphere interaction that is an integral part of the dynamical system to be modeled. Thus, in this respect a more satisfactory approach is to model the magnetosphere-ionosphere as a dynamical system which is autonomous under constant forcing. Such models can be constructed with varying degree of sophistication, [*Baker et al.*, 1990; *Klimas et al.*, 1992; *Horton and Doxas*, 1998], and may give rise to chaotic signals that reproduce many of the random characteristics of the magnetospheric time series. However, being deterministic and low-dimensional they cannot reproduce the strong stochastic component in the observational signals. On the other hand, such models can be generalized to include stochastic forcing from small-scale internal dynamics and deterministic and stochastic forcing from variations of the driver. Thus, one may conceive complicated as well as simple conceptual dynamic-stochastic models that can capture the essential stochastic dynamics as it presents itself in the observables studied here. In *Rypdal and Rypdal* [2010a, b] the AE index is modeled by a simple dynamic-stochastic equation that reproduces the general statistical features. The deterministic dynamics in this equation was represented by a drift term (a nonlinear damping) which prevents the solution to drift off to infinity, but the focus in those studies was on the time scales less than a 100 minutes, where the effect of the drift term is small. A version of this stochastic difference equation that exhibits on-off intermittency for certain choices of parameters is

$$\delta X = M(x)\delta t + \sqrt{D} X\, w \tag{10}$$

where $M(x) = aX - X^3$ with $a > 0$ models the drift term found from the AE index in *Rypdal and Rypdal* [2010b]. Here δt is the disrcrete time step (the sampling interval of the time series) and $\delta X(t) = X(t + \delta t) - X(t)$. In *Rypdal and Rypdal* [2010a] $w(t)$ is modeled as a particular multifractal stochastic noise process with unit variance. It was shown by *Aumaitre* [2005] that the on-off intermittency of this equation is sensitive to the nature of the noise term. If $w(t)$ is approximated by a white Gaussian noise, equation (10) in the limit $\delta \to 0$ reduces to the Itô stochastic differential equation

$$dX = (aX - X^3)\, dt + \sqrt{D}\, X dB(t),$$

where $B(t)$ is the Wiener process (Brownian motion). It can be shown from the associated Fokker-Planck equation that the stationary probability density for X is $P(X) = CX^{(2a/D)-1}e^{-(X^2/D)}$. The divergence of $P(X)$ as $X \to 0$ for $2a/D < 1$ is due to the on-off intermittency in this regime, which makes the solution reside in the vicinity of $X = 0$ for a considerable portion of the time, while for $2a/D - 1$ small, but positive, the solution has an intermittent character more similar to the behavior of the AE index. Such a solution is shown in Figure 10a, with a sample of the AE index shown in panel (b). Here w was chosen as a weakly anti-persistent fractional Gaussian noise with Hurst exponent $H = 0.45$, which is the H-value derived from the power spectral density for AE shown in Figure 11. The relation between the spectral index β, which is the slope of the straight lines fitted to the spectra plotted in a log-log plot, and the Hurst exponent of the differentiated signal is $\beta = 2H + 1$. On time scales < 100 time steps (minutes) AE index has $\beta \approx 1.90$, corresponding to $H \approx 0.45$. The power spectral density for the model signal shows a less clear power-law regime on these time scales, which is mainly due to a crude model for the nonlinear drift term $M(X)$ in equation (10). A more "box-like" function would remedy this. On time scales > 100 minutes the spectrum for the AE index has a pink-noise character ($\beta \approx 1$), while the model time series has a more gradual transition towards white noise. Further study on refinements of equation (10) is required to settle whether these spectral features are possible to reproduce within this class of one-dimensional stochastic equations.

An interesting question is whether modeling along these lines can produce bursts (substorms) which enhance the determinism compared to a completely random process. As discussed before, the test based on comparing the L_n-curve with the one obtained after randomization of phases is a test on the existence of a low-dimensional and nonlinear component in the dynamics. Direct computation of L_n from the model signal does not reveal a significant enhancement of L_n after randomization, in contrast to what was found from the MG system signal in Figure 1. One obvious reason for this is that the signal from equation (10) contains a strong stochastic component which is not present in the signal from the MG system. Hence, in this case it is necessary to perform a mild low-pass filtering of the model signal before computation of L_n. The result after filtering is shown in Figure 12, indicating the presence of a low-dimensional nonlinear component. To make sure that this filtering does not introduce spurious low-dimensional nonlinearities in the signal, we perform the same test to a filtered fO-U process with similar spectral characterics as our model signal (the power spectral density for the fO-U signal is displayed in Figure 11). The filtered fO-U process shows very small change of L_n after randomization of phases, as shown in the inset of Figure 12. Obviously, low-pass filtering also have an effect on this test when applied to physical signals with a stochastic component. In Figure 13 we show the effect of applying the same filter to tAE, which should be compared to the result for the unfiltered signal shown in Figure 5.

The nonlinearity producing determinism in the model signal from equation (10) is a combination of the nonlinear drift term and the multiplicative noise term $\sqrt{D}Xw$. The multiplicative term can be eliminated by the transformation $Y = \log X$, but then Itô's formula [*Gardiner*, 1985] yields a new drift term on the form $\tilde{M}(Y) = e^{-Y}M(e^Y) - D/2$. Note that if our original drift term is a linear damping $M(X) = -\nu X$ the transformed drift term reduces to a negative constant $\tilde{M}(Y) = -(\nu + D/2)$. This yields $Y(t) \to -\infty$, and hence $X(t) \to 0$ as $t \to \infty$, and demonstrates that the drift term must be nonlinear to produce stationary time series from a model with a multiplicative noise term like equation (10).

Acknowledgments. The authors acknowledge extensive discussions with M. Rypdal. Recurrence plot and the longest diagonal line are computed by means of the Matlab package downloaded from
`http://www.agnld.uni-potsdam.de/~marwan/toolbox/.`

References

Athanasiu, M. A., and G. P. Pavlos (2001), SVD analysis of the magnetospheric AE index time series and comparison with low-dimensional chaotic dynamics, *Nonlin. Processes Geophys.*,, *8*, 95.

Aumaitre, S., F. Pételis, and K. Mallick (2005), Low-Frequency Noise Controls On-Off Intermittency of Bifurcating Systems, *Phys. Rev. Lett.*,, *95*, 064101.

Bak, P., C. Tang, and K. Wiesenfeld (1987), Self-organized criticality: An explanation of 1/f noise, *Phys. Rev. Lett., 59*, 381.

Baker, D. N. , A. J. Klimas, R. L. McPherron, and J. Büchner (1990), The evolution from weak to strong geomagnetic activity: an interpretation in terms of deterministic chaos, *Geophys. Res. Lett, 17*, 41.

Chang, T. S (1999), Self-organized criticality, multi-fractal spectra, sporadic localized reconnections and intermittent turbulence in the magnetotail, Phys. Plasmas *6*, 4137.

Chapman, S., and N. Watkins (2001), Avalanching and self-organised criticality, a paradigm for geomagnetic activity, *Space Science Review*, *95*, 293.

Chapman, S. C., N. W. Watkins, R. O. Dendy, P. Helander, and G. Rowlands (1998), A simple avalanche model as an analogue for magnetospheric activity, *Geophys. Res. Lett. 25*, 2397.

Davies, T. N, and M. Sugiura (1966), Auroral electrojet activity index AE and its universal time variations, *J. Geophys. Res., 71*, 785.

Eckmann, J. P, S. O. Kamphorst and D. Ruelle (1987), *Europhysics Letters 5*, 973.

Feldstein, Y. I., V. A. Popov, J. A. Cumnock, A. Prigancova, L. G. Bloomberg, J. U. Kozyra, B. T. Tsurutanj, L. I. Gromova, and A. E. Levitin (2006), Auroral electrojets and boundaries of plasma domains in the magnetosphere during magnetically disturbed intervals, *Ann. Geophys., 24*, 2243.

Freeman, M. P., N. W. Watkins, and D. J. Riley (2000), Evidence for a Solar Wind origin of the power law burst lifetime distribution of the AE indices, *Geophys. Res. Lett*, *27*, 1087.

Frey, H. U., S. B. Mende, V. Angelopoulos, E. F. Donovan (2004), Substorm onset observation by IMAGE-FUV, *J. Geophys. Res., 109*, 10,304.

Gardiner , C. W. (1985) , Handbook of Stochastic Methods , Springer, New York.

Golovchanskaya, I. V. , B. V. Kozelov, T. I. Sergienko, U. Brändström, H. Nilsson, and I. Sandahl (2008), *J. Geophys. Res., 113*, A10303.

Horton, W, and I. Doxas (1998), A low-dimensional dynamical model for the solar wind driven geotail-ionosphere system, *J. Geophys. Res., 103*, 4561.

Kaplan, D. T., and L. Glass (1992), Direct test for determinism in a time series, *Phys. Rev. Lett.*, *68*, 427.

Klimas, A., D., D. N. Baker, D. A. Roberts, and D. H. Fairfield (1992), A nonlinear dynamical analogue model of geomagnetic activity, *J. Geophys. Res., 97*, 12253.

Kozelov, B. V., and T. V. Kozelova (2003), Cellular automata model of magnetospheric-ionospheric coupling, *Ann. Geophys., 2*1, 1931.

Lewis, Z. V. (1991), On the apparent randomness of substorm onset, *Geophys. Res. Lett., 1*8, 1627.

Mackey, M. C., and L. Glass (1977), Oscillation and chaos in physiological control systems, *Science*, *197*, 197.

March, T. K, S. C. Chapman, and R. O. Dendy (2005a), Recurrence plot statistics and the effect of embedding, *Phys. D*, *200*, 171.

March, T. K, S. C. Chapman, and R. O. Dendy (2005b), Mutual information between geomagnetic indices and the solar wind as seen by WIND: Implications for propagation time estimates, *Geophys. Res. Lett.*, *32*, L04101.

Marwan, N., M. C. Romano, M. Thiel and J. Kűrths (2007), *Physics Reports 438*, 237.

Rypdal, M., and K. Rypdal (2010a), Stochastic modeling of the AE index and its relation to fluctuations in B_z of the IMF on time scales shorter than substorm duration, *J. Geophys. Res., 115*, A11216.

Rypdal, M., and K. Rypdal (2010b), Discerning a linkage between solar wind turbulence and ionospheric dissipation by a method of confined multifractal motions, *J. Geophys. Res., 116*, A02202.

Sharma, A. S, D. Vassiliadis, K. Papadopoulos (1993), Reconstruction of low-dimensional magnetospheric dynamics by singular spectrum analysis, *Geophys. Res. Lett.*, *20*, 335.

Sitnov, M. I., A. S. Sharma, and K. Papadopoulos (2001), Modeling substorm dynamics of the magnetosphere: From self-organization and self-organized criticality to nonequlibrium phase transitions, *Phys. Rev. E, 65*.

Takens, F. (1981), Detecting strange attractors in fluid turbulence, in: Dynamical Systems and Turbulence , edited by D. Rand, and L. S. Young, Springer, Berlin.

Tsurutani, B., M. Sugiura, T. Iyemori (1990), The nonlinear response of AE to the IMF B_s driver: a spectral break at 5h, *Geophys. Res. Lett., 17*, 279.

Uritsky, V. M., A. J. Kimas, and D. Vassiliadis (2002), Multiscale dynamics and robust critical scaling in a continuum current sheet model, *Phys. Rev. E.*, *65*, 046113.

Uritsky, V. M., and M. I. Pudovkin (1998), Low frequency 1/f-like fluctuations of the AE-index as a possible manifestation of self-organized criticality in the magnetosphere, *Ann. Geophys.*, *16*, 1580.

Vennestrøm, S. , E. Friis-Christensen, O. A. Troshicev, and V. G. Andrezen (1991), Comparison between the polar cap PC and the auroral electrojet indices AE, AL and AU, *J. Geophys. Res., 96*, 101.

Vörös, Z. (1991), Synergetic approach to substorm phenomenon, in: Magnetospheric substorms, edited by Kan. J. R., Geophys. Monograph, *64*, 461.

Wanliss, J. A., and K. M. Showalter (2006), High-resolution global storm index: *Dst* versus SYM-H, *J. Geophys. Res., 111*, A02202.

Živković, T., and K. Rypdal, Low-dimensionality and predictability of solar wind and global magnetosphere during magnetic storms, submitted to J. Geophys. Res., http://dl.dropbox.com/u/12007133/Zivkovic%20and%20Rypdal-JGR-I.pdf

T. Živković, Department of physics and Technology, University of Tromsø, 9037 Tromsø, Norway (tatjana.zivkovic@uit.no)

K. Rypdal, Department of physics and Technology, University of Tromsø, 9037 Tromsø, Norway